



STScI | SPACE TELESCOPE
SCIENCE INSTITUTE

Instrument Science Report COS 2025-09(v1)

A Revised Geometric Distortion Correction for the Far-Ultraviolet Detector of the Cosmic Origins Spectrograph

Darshan Kakkad^{1,2}, Nick Indriolo^{1,3}, Tom Ake¹, John Debes^{1,3}, David French¹, Sten Hasselquist¹, David Sahnou¹, Charles Proffitt¹, Julia Roman-Duval¹

¹Space Telescope Science Institute, Baltimore, MD

²Centre for Astrophysics Research, University of Hertfordshire, Hatfield AL10 9AB, UK

³AURA for European Space Agency, STScI, USA

2 July 2025

ABSTRACT

We describe the derivation of a new geometric distortion correction reference file for the far-ultraviolet (FUV) detector of the Cosmic Origins Spectrograph (COS) aboard the Hubble Space Telescope (HST). The geometric distortion correction aims to achieve a uniform plate scale across both segments of the FUV detector by applying a transformation from thermally-corrected coordinates to a coordinate system where pixels measure $6\ \mu\text{m} \times 24\ \mu\text{m}$. The previous version of the geometric distortion correction reference file (GEOFILE) was known to have problems at some locations that negatively impacted the accuracy of fluxes and wavelengths in calibrated data products, hence the motivation to derive a new geometric distortion correction. To derive the distortion corrections in both the dispersion and cross-dispersion directions (dx and dy , respectively), we utilized Pt-Ne lamp spectra obtained during the Thermal Vacuum testing campaign in 2003. This process involved comparing the observed locations of individual emission lines from the Pt-Ne spectra with ray-trace models. Through interpolation and extrapolation we generated the reference file image arrays corresponding to the full active area of the detector. The new GEOFILE addresses previous artifacts and sub-optimal corrections, significantly enhancing performance across multiple detector regions in conjunction with newly implemented walk and delta-geometric corrections.

Contents

1. Introduction	2
2. Data	4
3. Analysis of TV03 data	6
3.1 Distortion Measurement	7
3.1.1 Line Positions and Assignment	7
3.1.2 Calculating the dx distortion	8
3.1.3 Calculating the dy distortion	10
3.2 GEOFILE creation	11
3.3 Iteration	13
3.4 Results	14
4. Validation Testing	14
4.1 Residual Errors	17
5. Summary	18
Acknowledgements	20
Change History for COS ISR 2025-09	20
References	20

1. Introduction

The Cosmic Origins Spectrograph (COS) on board the Hubble Space Telescope (HST) provides unique spectroscopic capabilities at far-ultraviolet (FUV) wavelengths. In the FUV, the COS instrument has both medium and low resolution spectroscopy modes via gratings G130M, G160M, and G140L, which provide simultaneous wavelength coverage from 900–1450 Å at $R \approx 12000$ –17000, 1360–1775 Å at $R \approx 13000$ –20000 and < 900–2150 Å at $R \approx 1500$ –4000, respectively.

The FUV detector is comprised of two spectrally aligned microchannel plate (MCP) segments (FUVA, FUVB) which record a user-selected part of the wavelength range of each grating. These segments are analog in nature; i.e., they do not have physical pixels. Incident photons are assigned to digital pixels by the electronics using a series of finely tuned steps, described briefly below. An electron released from the impact of a UV photon on the photocathode layer at the top of a detector segment travels down the MCP stack, initiating an electron cascade that ultimately reaches the anode beneath the MCP stack as a charge cloud.¹ This produces electronic pulses that travel in opposite directions down two cross-delay lines (XDL), one of which is oriented in the dispersion (x) direction, and one of which is oriented in the cross-dispersion (y)

¹For graphical representations of this process, see, e.g., Wiza (1979)

direction. The difference in the arrival times of the signals at the opposite ends of each XDL determine the digital pixel assignment along that axis within an array of size 16384×1024 ($x \times y$). To measure the arrival time of a pulse accurately, each pulse is passed through a constant fraction discriminator (CFD). The CFD makes a time-delayed copy of the original pulse and subtracts that copy from the original pulse, resulting in an output pulse that has a zero-crossing (see Vallerga & McPhate 2000, Figure 5). Using this method, the location of this zero-crossing is independent of the pulse amplitude, and so the zero-crossing point is used to measure the pulse arrival time. The amplitude of the pulse is also saved in a 5-bit number (0–31) referred to as the pulse height amplitude (PHA), which carries information about the gain of the detector at that location. The CFD produces a zero-crossing point that is independent of pulse amplitude, but not pulse width. As pulses travel down the XDLs they expand, such that a pulse originating on one side of the detector will have a different width than a pulse originating on the other side of the detector. This pulse expansion, coupled with ripples in the baseline caused by signal reflections within the electronics, results in the zero-point crossing moving within the CFD output pulse (Vallerga & McPhate 2000). This effect, along with variable signal speeds in the XDLs caused by localized variations in the properties of the anode substrate, causes the physical size of a region on the MCP associated with a digital pixel to vary across the detector (i.e., a non-uniform plate scale), an effect known as integral non-linearity or geometric distortion (Vallerga et al. 2001; Wilkinson et al. 2001). The COS geometric distortion is only a function of position (x and y). Movement of recorded photons as a function of PHA is another effect called walk, and is discussed in the accompanying documents Hasselquist et al. (2025a) and Hasselquist et al. (2025b).

The CalcCOS pipeline performs a correction for the geometric distortion during the GEOCORR step, the purpose of which is to move photon events from the distorted pixel arrays returned by the detector segments to arrays where digital pixels have uniform sizes ($6 \times 24 \mu\text{m}$). This step follows the temperature-dependent distortion correction (TEPCORR), and so operates on data in the thermally-corrected coordinate system (XTHERM, YTHERM). Corrections are stored in the GEOFILE reference file in four image extensions (dx and dy corrections for both FUV A and FUV B), and are defined as $dx = \text{XTHERM} - \text{XCORR}$ and $dy = \text{YTHERM} - \text{YCORR}$. The previous version of the geometric distortion correction reference file (`x1u1459gl_geo.fits`) was created during ground testing, and has been applied to on-orbit data since the installation of COS on HST in 2009. While this correction works well at the original location on the detector where spectra were recorded (Lifetime Position 1, or LP1 for short), the expansion of observations to other cross-dispersion locations has revealed some problems with the correction at other LPs. This includes wavelength errors being introduced by the previous GEOFILE in the LP4 region of FUV A, as well as artificial flux deficits near both edges of FUV B (known as grid wire impostors; Osten et al. 2013). Because of these issues, the decision was made to re-derive the FUV geometric distortion correction for COS, and thus remove the artifacts being introduced by the previous correction. As part of this effort, walk in both the x and y directions has also

been measured, and new reference files to correct X-walk and Y-walk delivered. An overview of this entire project can be found in Indriolo et al. (2025a), along with more detailed descriptions of the issues that motivated the need for a new geometric distortion correction.

2. Data

Initial measurement of the geometric distortion of the COS FUV detector is described in Béland et al. (2003), but a partial disassembly of the unit changed the physical characteristics of the detector enough to render that correction invalid. The subsequent measurement of the geometric distortion (which produced the previous reference file) relies on a ray-trace analysis of the HST+COS FUV optics and grating (Béland & Penton 2000), and is described in Béland & Penton (2006) and Béland et al. (2007). This method uses the ray-trace model to predict the physical locations of emission lines with known wavelengths on the detector, and determines the shift necessary to move those lines from a thermally-corrected digital pixel array to a new geometrically-corrected digital pixel array with a uniform plate scale. The data required for this analysis were obtained as part of the Thermal Vacuum testing campaign in October 2003, and will be referred to as the TV03 data set herein. The TV03 data set consists of 112 individual Pt-Ne emission line spectra observed using the G160M/1600 setting. In the region of the detector accessible by the wavelength calibration aperture (WCA), spectra were produced by the Pt-Ne hollow cathode lamp on the internal COS calibration platform, and were observed at 13 different cross-dispersion locations. In the region of the detector accessible by the primary science aperture (PSA), spectra were produced by an external Pt-Ne hollow cathode lamp that was part of the Calibration Delivery Subsystem and fed light into the Reflective Aberration Simulator for CALibration (RASCAL), which simulated the HST optics before passing the beam into the COS aperture (Wilkinson et al. 2008). Pt-Ne spectra were observed through the PSA using this system at 15 different cross-dispersion locations. At all cross-dispersion locations sampled by the WCA and PSA, all four FP-POS of cenwave 1600 were used to shift the emission lines on the detector in the dispersion direction, and thus increase the sampling in the x-direction. Figure 1 summarizes the full extent of the TV03 data set on both detector segments by adding together thermally-corrected `flt` images from all 112 exposures. A zoomed-in view of select exposures, along with their corresponding spectra, is presented in Figure 2.

To re-measure the COS FUV geometric distortion we use the same TV03 data set that was used to produce the previous reference file. The original analysis excluded the four exposures taken through the PSA at the lowest YTHERM location due to minor complications discussed later (see Section 3.1.3), but we include these exposures to extend the region on the detector with measured (rather than extrapolated) distortions slightly lower, important for data taken at LP4. We also use new software routines

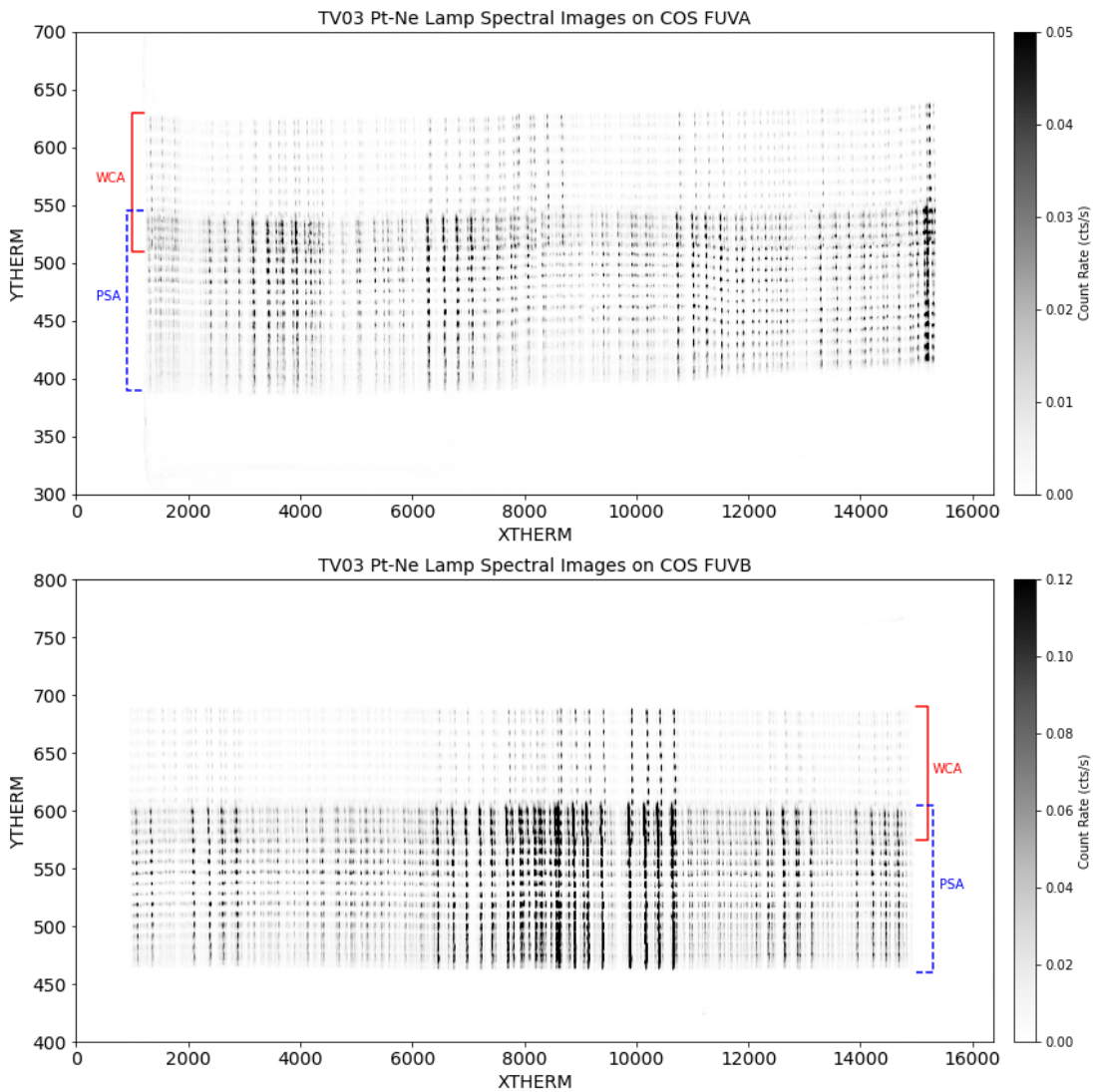


Figure 1. This is the combination of all `flt` images corresponding to 112 exposures taken with spectra located at different cross-dispersion locations and FP-POS for segment FUVA (top) and FUVB (bottom). Regions covered by the WCA and PSA are marked. Each “row” of emission lines comes from four separate exposures at FP-POS=1, 2, 3, and 4.

that account for the changing line profiles and blended emission lines shown in Figure 2. Finally, we pay special attention to regions where we know the previous geometric distortion correction introduced artifacts (e.g., Indriolo et al. 2025a Figures 1 and 2), identifying errors within that GEOFIL and making sure they do not appear in our new version.

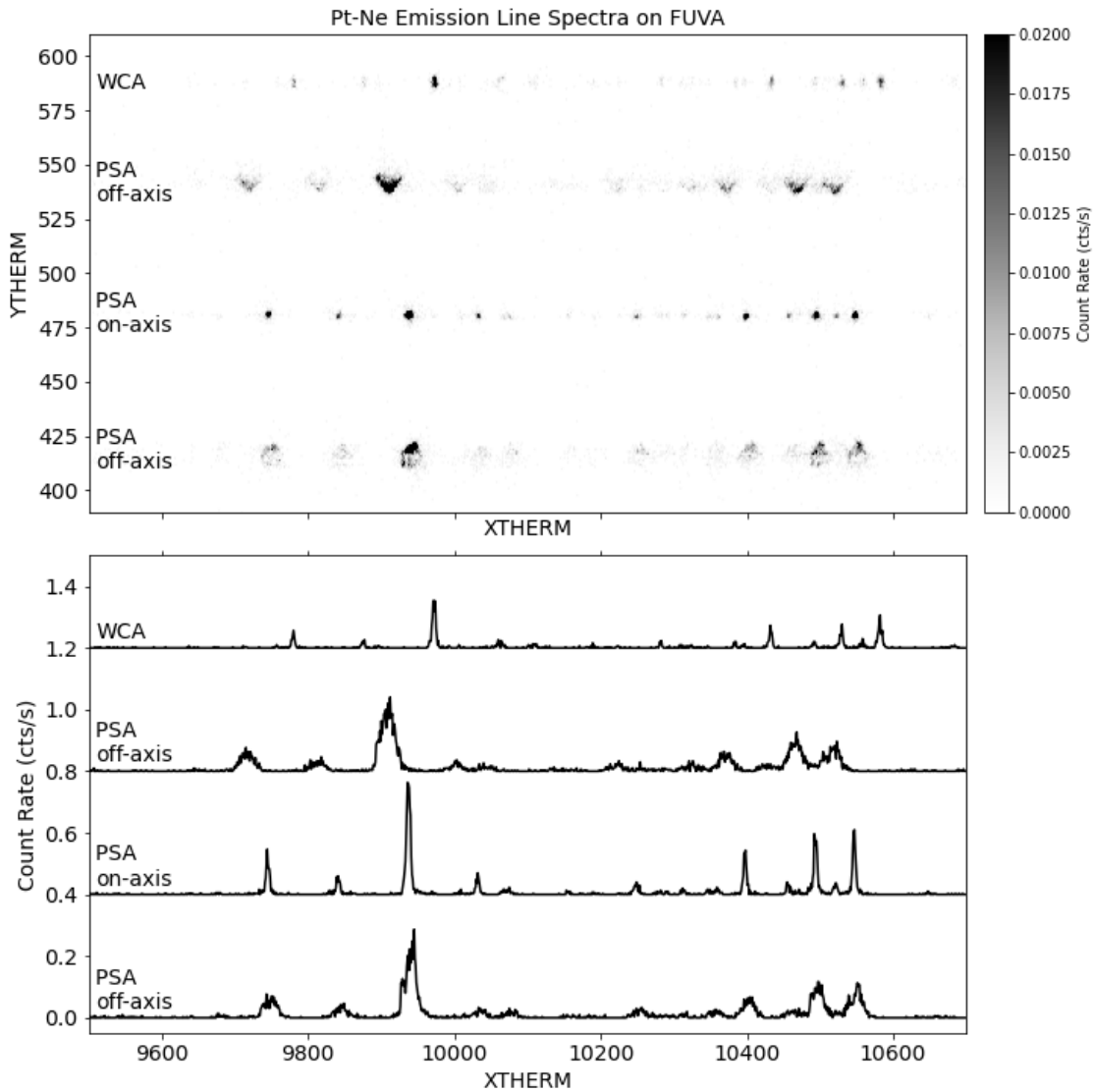


Figure 2. The top panel shows part of a combined 2D image of 4 representative exposures out of the full TV03 data set on FUVA. The top-most spectrum was observed through the WCA, and the other three through the PSA. Because the focus was not changed during this observing sequence, the two off-axis PSA spectra have distorted profiles compared to the on-axis PSA spectrum. The bottom panel shows the 1D spectra extracted from the exposures in the top panel, shifted vertically for clarity and to be in the same sequence. Due to the changing line profiles and blending of emission lines, the number of measurements and the uncertainty on those measurement varies as a function of position on the detector.

3. Analysis of TV03 data

Creation of the geometric distortion correction reference file consists of two main steps. First, the distortions in both the x and y directions are measured for each Pt-Ne

line (or group of blended lines) by comparing the line centers in the thermally corrected images to the expected location in physical space. This produces a set of measured distortions, dx and dy , at discrete locations (X THERM, Y THERM) on the detector. Second, the measured distortions are interpolated onto a 2D image array that corresponds to a portion of the full 16384×1024 coordinate space for each segment, and then extrapolated to a rectangular region that roughly corresponds to the active area of the detector. This is done separately for the dx and dy corrections on each detector segment, resulting in four correction images. These are stored separately as the four data extensions in the GEOFILE, and the extension headers provide information about the rectangular region covered by that image in the keywords ORIGIN_X and ORIGIN_Y (lower left corner of the region) and NAXIS1 and NAXIS2 (size of the region in the x and y directions, respectively).

3.1 Distortion Measurement

Measurement of the geometric distortion can be further broken down to measuring the positions of emission lines, identifying and assigning wavelengths to those lines, predicting the locations where those lines should appear in a uniform digital pixel grid, and computing the difference between the observed and predicted locations.

3.1.1 Line Positions and Assignment

As described earlier, the TV03 data set consists of a series of 112 Pt-Ne spectra. While combined into a single image for display purposes in Figure 1, the spectra are analyzed one at a time for the purpose of measuring line positions. To perform this analysis, we use a set of IDL codes that was originally designed to measure a delta-geometric correction (small-scale correction in addition to the already applied geometric distortion correction), and which operates on geometrically corrected data. Using data that have been partially processed with CalcOS has the advantages of making line identification easier², allowing for joint fitting of closely spaced or blended lines, and enabling the use of data quality (DQ) flags to exclude potentially bad measurements (Soderblom et al. 2022), but requires a back-conversion from CORR to THERM coordinates once the positions are measured. To prepare the data for analysis, the raw files are run through CalcOS with the FLATCORR, DQICORR, TEMPCORR, GEOCORR, IGEOCORR, RANDCORR, and PHACORR steps set to PERFORM. This produces the flat images in geometrically corrected space on which the IDL analysis code operates.

For each exposure the relevant region of the flat image is collapsed into a 1D spectrum and DQ array. Using a list of Pt and Ne transition wavelengths and intensities derived from laboratory measurements (Sansonetti et al. 2003) and assuming gaussian line shapes, a model spectrum is generated over the expected wavelength range

²Wavelengths assigned by the initial pipeline processing, even if not perfect, simplify comparison between the observed and modeled spectra.

covered by the exposure. The model spectrum is fit to the observed spectrum over the entire segment. This serves to determine the average FWHM of lines in the spectrum, and to roughly identify³ the emission features in the observed spectrum. The best-fit model spectrum is then separated into windows in XCORR that contain either individual emission lines or blends of emission lines. Within each window, a refined fit of the model to the data is performed to better match the observed line parameters. This step is repeated to further refine the fits, and the result of this process is that all emission lines in the spectrum are assigned a wavelength and an XCORR location. Taking the same XCORR windows defined above, the 2D spectrum in the `flt` image is collapsed in the x-direction to create a cross-dispersion profile within the window. The flux-weighted centroid of this cross-dispersion profile is calculated, and is taken to be the YCORR location of the emission line(s) within that window. This process is repeated for all exposures on both detector segments, producing a set of measurements that contain XCORR, YCORR, wavelength, and any DQ flags associated with the data for all emission lines within the TV03 data set.

As previously mentioned, the geometric distortion correction operates on data in the thermally-corrected coordinate system, so the (XCORR, YCORR) values determined above must be converted to (XTHERM, YTHERM) coordinates before the distortion can be measured. This is done by “reversing” the geometric distortion correction that was applied to the TV03 data set during our initial processing with CalcOS. Using the GEOFILE dx and dy images and the (XCORR, YCORR) coordinates, we iteratively remove the approximately applied corrections until converging on the location in (XTHERM, YTHERM) where the dx and dy corrections would move an event to the measured (XCORR, YCORR) location. In this way, we determine the (XTHERM, YTHERM) positions of the identified emission lines, and can use these data to measure geometric distortions.

3.1.2 Calculating the dx distortion

To measure the geometric distortion, we follow the methodology developed by the COS Instrument Development Team (IDT), provided by Béland (2004) (private communication). This process involves mapping the locations of Pt-Ne emission lines on the detector between four different coordinate systems: wavelength (λ), physical space (p), thermally corrected pixel space (x or x_{therm}), and geometrically corrected pixel space (x_{geo}). The estimated locations for the Pt-Ne lines in physical space (p , in mm) are calculated by inverting a ray-trace model (equation 1) that yields wavelength (λ , in Å) as a function of position from the center of the gap between the segments for CENWAVE=1600, FP-POS=3:

$$\frac{\lambda}{1600} = 0.99828943 - 0.00127483p + 6.0961841 \times 10^{-10}p^2 + 3.0525757 \times 10^{-12}p^3. \quad (1)$$

³Due to distortions, the observed and model emission lines will not be aligned across the whole segment, hence rough identification here.

The negative linear dispersion term indicates that p here is defined in the pre-launch coordinate system⁴. Equation 1 yields the wavelength corresponding to a given position in p , but we instead need to predict p locations corresponding to Pt-Ne emission line wavelengths. To do this, we empirically invert the cubic polynomial of Equation 1. The result is

$$p = \delta p + 784.51990 - 0.49278884\lambda + 1.4673714 \times 10^{-6}\lambda^2 - 2.8223787 \times 10^{-10}\lambda^3, \quad (2)$$

where λ is the vacuum wavelength of a Pt-Ne line and δp is +47 for FUVB and -47 for FUVB. These δp offsets arise because in determining the geometric distortion for each segment, we need to transform the inverted polynomial into a coordinate system centered at each segment individually. Since the active area of each detector segment is 85 mm long with a gap between the segments of 9 mm, we modify the inverted zero-point by +47 mm for FUVB and -47 mm for FUVB for the analyses. Using equation 2, we can then predict the physical locations of Pt-Ne emission lines on each detector segment.

However, the use of different FP-POS and non-repeatability of the Optics Select Mechanism 1 (OSM1) mean that all of the observed spectra will be shifted in the dispersion direction with respect to the location predicted by equation (2). As a result, we must determine the offset in physical space between the inverted ray-trace model prediction and each individual spectrum, and remove it before calculating dx distortions. For each segment, the center of pixel $x = 8192$ is defined to be at the physical location $p = 0$ mm, and to have no distortion ($dx = 0$). We identify the two closest measured emission lines on either side of pixel 8192, and use their predicted physical and measured pixel locations to compute a local plate scale (in mm/pixel). With this plate scale we determine the physical distance between pixel 8192 and the closer of the two emission lines, which serves as a new predicted physical location (p_{new}) for this particular emission line. The difference between originally predicted and newly predicted physical locations ($p - p_{new}$), represents the offset between the observed spectrum and the inverted ray-trace solution. By subtracting this offset from all of the originally predicted physical positions, we generate new predicted locations for all emission lines in physical space. Using these new predicted locations, and adopting a uniform plate scale of $6.0 \mu\text{m}/\text{pixel}$, we define the locations of these emission lines in geometrically corrected pixel space as:

$$x_{geo} = \frac{p_{new}}{-0.006} + 8192, \quad (3)$$

where the negative sign for the plate scale converts the pixels back from the detector to the user coordinate system. The geometric distortion in the x-direction is then computed as the difference between the measured location of an emission line in thermally corrected pixel space and the predicted location of an emission line in geometrically corrected pixel space: $dx = x_{therm} - x_{geo}$.

⁴Conversion between the detector coordinate system and user coordinate system is given by $x_{user} = 16383 - x_{detector}$ and $y_{user} = y_{detector}$; see Section 1.4 in Soderblom et al. (2022) for more details.

3.1.3 Calculating the dy distortion

To measure geometric distortions in the y -direction we again adopt the methods and measured properties⁵ of the instrument used by the COS IDT (Béland 2004, private communication). The predicted physical location of a spectrum taken through the PSA is based on the position of the aperture mechanism in the cross-dispersion direction (LAPXSTP), projected on the detector. We define there to be no distortion in the y -direction ($dy = 0$) at the location of best focus for the TV03 PSA data (LAPXSTP = 147.1). For the WCA exposures, the LAPXSTP value is adjusted to account for the offset between the PSA and WCA. In the TV03 data set, each “row” of four spectra were taken about 20 aperture mechanism steps apart, except for the one furthest towards the bottom of the detector, which was only 7 steps below the row above it.⁶ Despite the smaller separation between aperture mechanism positions, the mirror in the RASCAL system was tilted at an angle corresponding to the full 20 step separation, meaning that the beam passed through the PSA 0.62” below center, and still projected to a location on the detector where the spacing between this row of data and the row above it is the same as between all other rows. No vignetting or other effects were found in these spectra, so the data were used in the new dx and dy distortion calculations.

Each cross-dispersion step of the aperture mechanism corresponds to a movement of $13.26 \mu\text{m}^\dagger$. With a demagnification factor of 0.9499^\dagger to the detector, defining a uniform pixel size of $24 \mu\text{m}$, and assuming a linear solution, the geometrically corrected y -location of a spectrum (in pixels) taken through the center of the PSA, y_{geo}^{PSA} , is given by:

$$y_{geo}^{\text{PSA}} = y_0 - (\text{LAPXSTP} - 147.1) \times \frac{13.26 \times 0.9499}{24}, \quad (4)$$

where $y_0 = 478$ for FUV A and 536 for FUV B impose the $dy = 0$ at LAPXSTP = 147.1 condition. The WCA and PSA are offset from each other in the cross-dispersion direction (i.e., the two apertures project spectra to different locations on the detector for the same LAPXSTP position), so an offset must be added to the LAPXSTP value to predict where WCA spectra fall on the detector. Based on the overlapping PSA and WCA spectra in the TV03 data set, this separation was determined to be $2600 \mu\text{m}^\dagger$. For the WCA then, the predicted y -location (in pixels) of a spectrum in geometrically corrected space is:

$$y_{geo}^{\text{WCA}} = y_0 - \left(\text{LAPXSTP} - 147.1 - \frac{2600}{13.26} \right) \times \frac{13.26 \times 0.9499}{24} \quad (5)$$

As in the x -direction, the distortion in the y -direction is computed by taking the difference between the measured location of an emission line in thermally corrected pixel space and the predicted location of an emission line in geometrically corrected pixel space:

$$dy = y_{\text{therm}} - y_{geo}^{\text{WCA}}, \quad (6)$$

⁵Values marked with \dagger are from Béland (2004, private communication).

⁶This is the row of data that was discarded during the initial GEOFILE creation.

or

$$dy = y_{\text{therm}} - y_{\text{geo}}^{\text{PSA}}. \quad (7)$$

Note that this correction assigns a single y_{geo} location to the spectrum across the whole detector segment, so spectral profiles in geometrically corrected space should run parallel to the x-axis of the detector.

3.2 GEOFILE creation

As mentioned above, GEOFILE stores the dx and dy corrections as 2D image arrays that roughly correspond to the active area of the detector. To create these image arrays, we must interpolate between, and extrapolate from, the discrete locations (XTHERM, YTHERM) where the individual dx and dy measurements were made. Several methods of simultaneous 2D interpolation were considered for this purpose, but were ultimately rejected due to poor performance. Instead, we decided to perform two successive 1D interpolations, first in the x-direction, and then in the y-direction. Note that the following procedure is done separately for the dx and dy corrections on FUVB and FUVB.

Before starting the fitting procedures, potentially bad measurements must be excluded from the data set. This is done using the DQ flags associated with each measurement, which were saved as part of the process described in Section 3.1.1. Inspection of the measurements showed that emission lines falling on regions of the detector defined as a “low response region” (DQ = 1024) or “very low response region” (DQ = 16) frequently appear as outliers in terms of the magnitudes of dx and dy . In flat field images of the detector these regions appear as small “holes” of order tens of pixels in diameter, surrounded by rings of higher flux. Photons that should be recorded within a “hole” are instead pushed to the outer circumference⁷, so an emission line falling in such a region will be measured in the wrong place. Because of this issue, any measurements made from regions on the detector with DQ = 1024 or DQ = 16 are excluded from further analysis.

For interpolation in the x-direction, each “row” of four interleaved FP-POS exposures at a given cross-dispersion location is treated separately. The YTHERM locations of the individual measurements in that row are ignored, and dx (or dy) as a function of XTHERM is fit using a cubic spline function⁸. The locations of nodes in the spline fit are based on the density of data points in the x-direction, with each node separated by 4 data points. This spline fit extends from the XTHERM location of the first measurement on the left side of the detector segment, to that of the last measurement on the right side of the segment. Beyond this region, we extend the fit to the edge of the segment active area via linear extrapolation, with the slope of the line defined by the first (or last) two points within the spline fit. An example of this

⁷The exact cause of such features is beyond the scope of this document.

⁸We use the LSQUnivariateSpline class in `scipy.interpolate`.

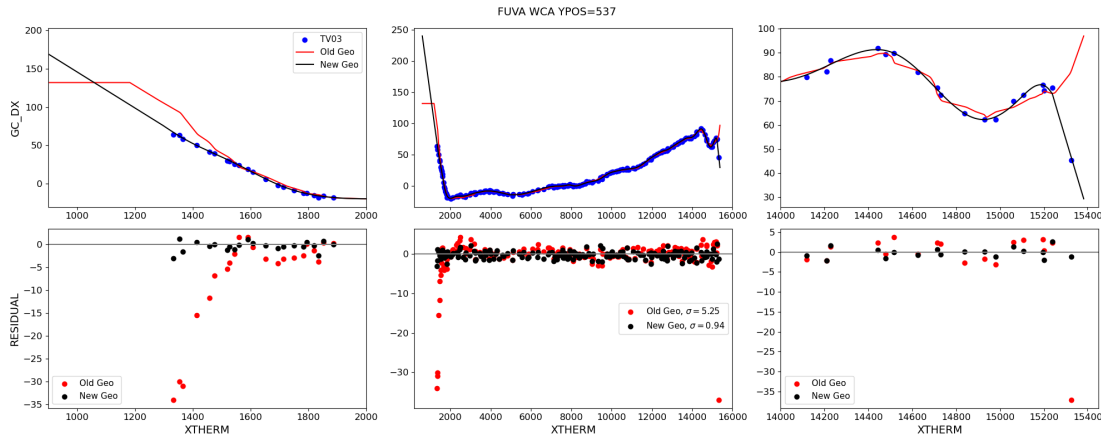


Figure 3. This is an example of the cubic spline interpolation in the x-direction for the dx distortion on FUVA at $YTHERM = 537$. The center column shows the full extent of the detector segment, while the left and right columns zoom in on the left and right edges of the segment, respectively. In the top row, blue points are the measured dx values plotted as a function of $XTHERM$. The black curve is the spline fit to those data points, while the red curve shows the correction at this location in the previous GEOFIL (`x1u1459g1_geo.fits`). In the bottom row, black points mark the residuals between the measurements and the new spline fit, while red points mark the residuals between the measurements and the previous dx correction.

procedure is shown in Figure 3 for the dx correction on FUVA at $YTHERM = 537$. This process is repeated for all 15 PSA and 13 WCA cross-dispersion locations where spectra were recorded, producing 28 spline fits, each of which is assigned a single $YTHERM$ location based on the average $YTHERM$ value of all measurements within that row. However, the region on the detector where PSA and WCA spectra overlap turned out to be problematic for the y-interpolation discussed below, so we chose to exclude the spline fits to the PSA data in this region (top four PSA rows) from the analysis going forward. This limits the data to 24 cross-dispersion locations, all of which are separated by roughly the same distance.

Interpolation in the y-direction uses the results of the x-direction spline fits as the new “measurements”. For a single value of $XTHERM$, the dx (or dy) value from each x-direction spline fit, and the $YTHERM$ location of that row are taken as the dependent and independent variables, respectively, and another cubic spline fit is performed. The spacing between nodes for this fit was 10 data points. Extrapolation above (below) the top (bottom) row of data to the edge of the active area is done using a constant value, equal to the last (first) point within the spline fit. An example of this procedure is shown in Figure 4, for the dy correction on FUVA at $XTHERM = 4000$. This is repeated for all $XTHERM$ values over which the x-direction spline fit plus extrapolation were defined, effectively filling the columns of a 2D dx (or dy) image array. These image arrays are the newly derived dx and dy corrections for FUVA and FUVB that can be

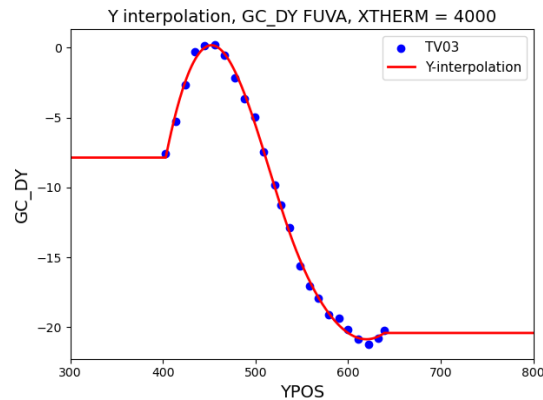


Figure 4. This is an example of cubic spline interpolation in the y -direction, for the dy correction on FUVA at $XTHERM = 4000$. Blue points mark the dy values determined at $XTHERM = 4000$ via the spline fitting in the x -direction. The red curve is the spline fit in the y -direction to the points.

used in the creation of a new GEOFILE.

3.3 Iteration

As described in Section 1, the COS FUV geometric distortion correction only depends on the locations x and y . Shifts due to different gain levels (PHA) are treated by the walk correction. The modal gain of the COS FUV detector varies with location, so the TV03 data set is not immune to walk. Separating the effects of geometric distortion from walk requires iteratively solving for the two (Indriolo et al. 2025a), with each iteration using the most recent reference files derived for the other correction. Once initial X- and Y-walk corrections were ready (Hasselquist et al. 2025a,b) the calibration switches XWLKCORR and YWLKCORR were set to PERFORM when using CalCOS to process the TV03 data. This produced a version of the data with the effects of walk removed, and the entire procedure of distortion measurement and reference file creation described above was repeated.

The overall procedure is nearly identical between iterations, with the sole difference being the conversion from $(XCORR, YCORR)$ to $(XTHERM, YTHERM)$ for measured line positions. The measured $(XCORR, YCORR)$ location of a Pt-Ne line in these data includes correction for both geometric distortion and walk. We need to remove the geometric distortion correction while retaining the walk correction, so that the measurement in $(XTHERM, YTHERM)$ coordinates is walk-corrected. The previously described conversion process uses $(XCORR, YCORR)$ as input to iteratively find and remove the dx and dy geometric distortion corrections that were applied to the data. This procedure no longer works for data that have been walk-corrected. To determine the actual dx and dy corrections that were applied, we take advantage of the

fact that the GEOCORR step occurs before the XWLKCORR and YWLKCORR steps within CalCOS. Both the initial iteration of our analysis (with no walk corrections applied) and subsequent iterations (with walk corrections applied) are measuring the same set of Pt-Ne emission lines from data that have had the same geometric distortion correction applied. We use the measured (XCORR, YCORR) location from data with no walk correction to determine the dx and dy geometric distortion corrections applied for a given emission line in *both* data sets. We then identify the same emission line in the walk-corrected data set, and remove the dx and dy corrections found above from that measured (XCORR, YCORR) location to produce a measured (XTHERM, YTHERM) location that has been corrected for walk. By removing walk from the TV03 data, we ensure that we are measuring only the effects of geometric distortion, with no contribution from walk. Because the initial walk corrections are not perfect though (the data sets used to measure X- and Y-walk suffer from geometric distortion), it is necessary to iterate between the two to separate their effects.

3.4 Results

In the end, we performed two full iterations between deriving the geometric distortion correction and walk corrections. The final GEOFILE correction images obtained from this analysis are shown in figures 5 and 6. Similar figures for the original FUV dx and dy corrections can be found in Béland & Penton (2006) or Béland et al. (2007), for comparison.

4. Validation Testing

An important step in determining that we had completed an iteration in updating the GEOFILE was to confirm that the new dx and dy corrections improve COS FUV data products with respect to the results from the previous iteration. This included checking that (1) the errors and artifacts mentioned in Section 1 (and described in more detail by Indriolo et al. 2025a) had been removed; (2) no new artifacts had been introduced to the data; and (3) the new correction performed as well as or better than the previous correction across the entire detector. If the GEOFILE being tested failed any of these checks, we investigated details of the analysis process (e.g., spline fitting parameters, extrapolation methods, etc.) to identify the underlying cause and generate a new GEOFILE with the issue removed, upon which the tests were repeated.

Validation of the dx correction relies on two tests: analysis of the distribution of wavelength residuals in emission/absorption line spectra, and analysis of the flux level in continuum spectra. The analysis of wavelength residuals is a key part of the overall effort to improve the geometric distortion and walk corrections, and is described in detail by French et al. (2025). The concept is simple; COS FUV dispersion solutions

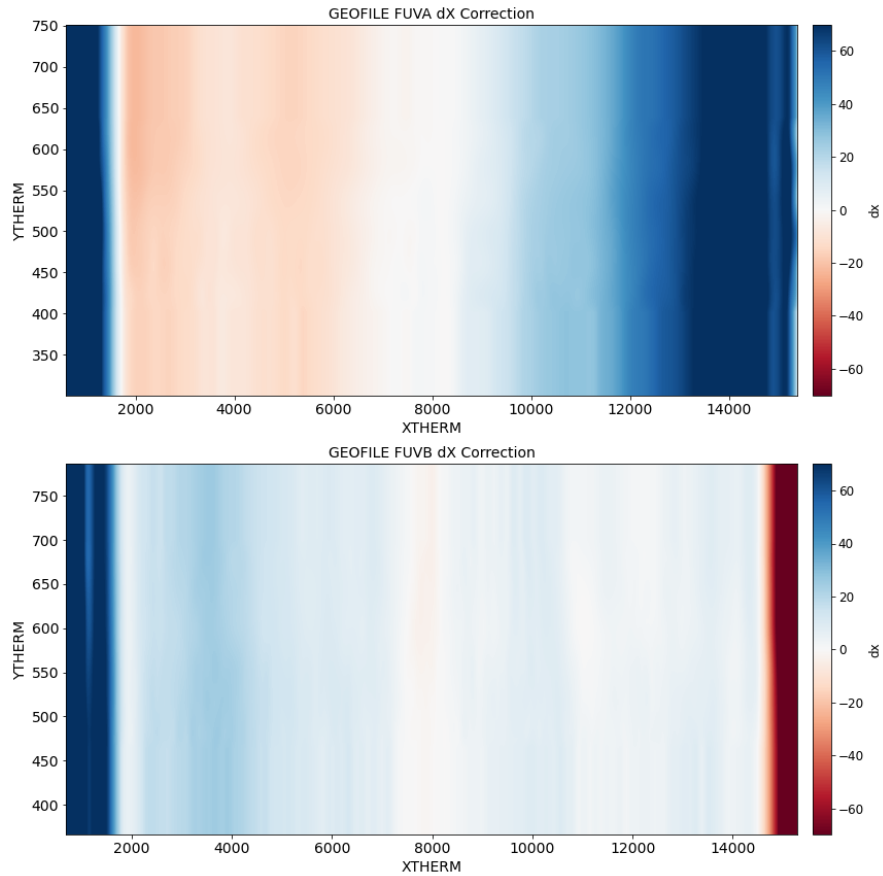


Figure 5. These are the final geometric distortion correction dx image arrays for FUVA (top) and FUVB (bottom).

for medium resolution gratings are linear⁹, such that $\lambda = a_0 + a_1 \times XFULL$. We compare the wavelength assigned to an emission (or absorption) feature by the dispersion solution to the known wavelength of that feature, and the difference between the two is assumed to be due to residual errors in the geometric distortion and X-walk corrections. We can look at these residuals for the same data set processed with the previous geometric distortion correction and the new geometric distortion correction, and the width of this distribution should decrease for an improved correction. An example of this analysis is shown in Figure 7. It is clear that data processed with our new geometric distortion correction show decreased residuals ($\sigma_{new} = 1.37$) compared to data processed with the previous geometric distortion correction ($\sigma_{old} = 2.46$), confirming that the new dx correction is an improvement over the previous correction. This test was repeated at all cross-dispersion locations on the detector where PSA and WCA spectra are routinely observed.

⁹While Equation 1 uses a cubic relation, the maximum deviation from a linear relation over the relevant wavelength range amounts to 0.25 pixels.

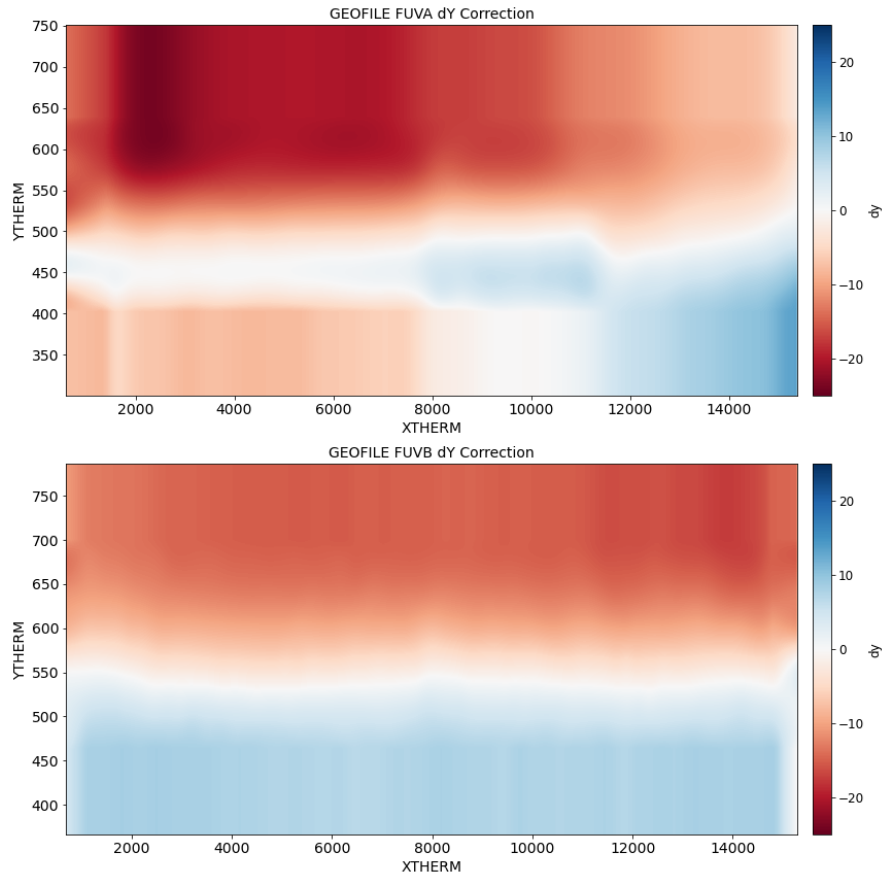


Figure 6. These are the final geometric distortion correction dy image arrays for FUVA (top) and FUVB (bottom).

Checking the flux level in continuum spectra is useful for identifying artifacts introduced by the geometric distortion correction. Features known as the grid wire impostors (Osten et al. 2013) near the left and right edges of FUVB are known to be caused by the previous geometric distortion correction. The dx correction at these locations changes rapidly with X THERM, resulting in counts being spread out across too many pixels, such that spectra have artificial flux deficits at these locations. Figure 8 compares the previous and new dx corrections at the locations where the grid wire impostors appear, demonstrating that the features in the previous GEOFILE that cause these artifacts have been removed in the new GEOFILE. It also shows that the flux deficits no longer appear in data processed with the new correction, again demonstrating that the new dx correction is an improvement.

In validating the dy correction, we consider how straight spectral profiles are across the detector. This is done by calculating the flux-weighted centroid in every X CORR column, as shown in Figure 9. Here, the red and blue curves correspond to the same original data set, but processed using the new and previous geometric

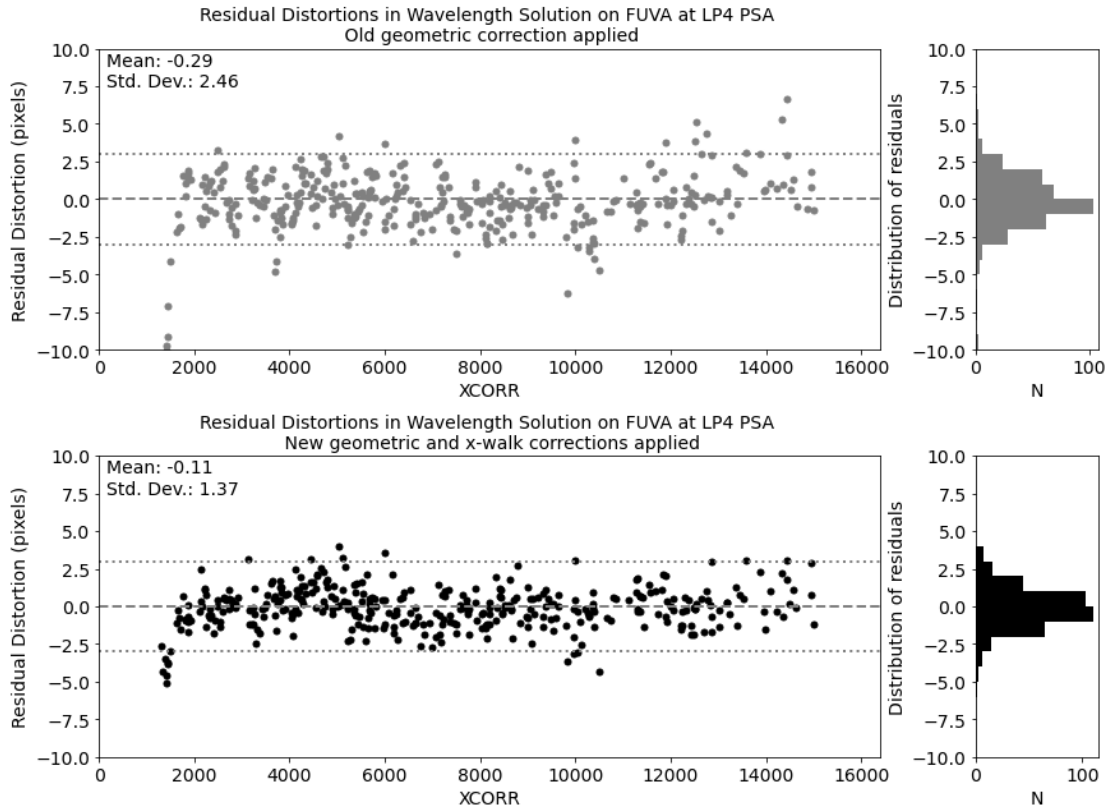


Figure 7. Residual shifts (in pixels) between the measured and predicted locations for emission lines in the spectrum of ϵ Eri observed on FUV A at LP4. The top panel shows the results from data processed with the previous GEOFILE, while the bottom panel shows the results from data processed with our new GEOFILE and the new X-walk correction.

distortion corrections, respectively. The centroid of the data processed using the new geometric distortion correction is clearly straighter across the detector, with standard deviations of $\sigma_{FUV A}^{new} = 0.33$ pixels and $\sigma_{FUV B}^{new} = 0.35$ pixels, compared to the original $\sigma_{FUV A}^{old} = 0.99$ pixels and $\sigma_{FUV B}^{old} = 0.47$ pixels. This test was performed at all cross-dispersion locations on the detector where spectra are routinely observed, confirming that the new dy correction performs as well as or better than the previous correction.

4.1 Residual Errors

The results presented in Figures 7–9 demonstrate that the combination of the new geometric distortion and walk corrections significantly improve COS data products. However, during the iterative effort to separate the effects of geometric distortion and walk into their respective reference files we discovered that some coherent structures within the wavelength residuals could not be removed by either the new geometric

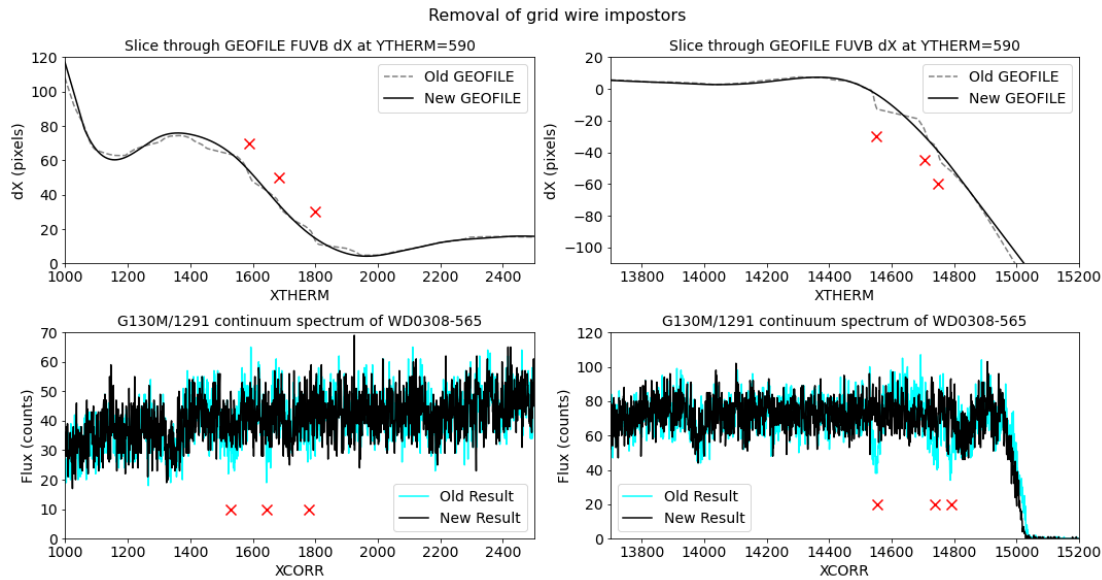


Figure 8. The top panels show the dx correction at $YTHERM = 590$ near the left and right edges of FUVB. Black curves and dashed grey curves are the new and old dx corrections respectively. Red crosses mark the features giving rise to grid wire impostors in the old reference file, and it is clear these have been eliminated in the new reference file. The results of processing data with the new correction are shown as black curves in the bottom panels, while data processed with the old correction are shown in cyan. The flux deficits caused by the grid wire impostors have been removed, demonstrating an improved dx correction.

distortion or new X-walk corrections (see Indriolo et al. 2025a for more details). Figure 10 shows an example of these residual errors that remain after application of the new geometric distortion and walk corrections. To further improve data products, we elected to employ a delta-geometric correction (small-scale correction after the initial geometric distortion correction) for the purpose of removing these residual errors. Details regarding the delta-geometric correction are beyond the scope of this document, and can be found in Indriolo et al. (2025b).

5. Summary

As part of the overall project to improve the geometric distortion and walk corrections on the COS FUV detector, we have created a new geometric distortion correction reference file. This new file has revised corrections for both dx and dy on FUVA and FUVB, and explicitly addresses known problems with the old correction, removing flux and wavelength artifacts that were being introduced into calibrated data products. Validation testing of the new geometric distortion correction combined with the new

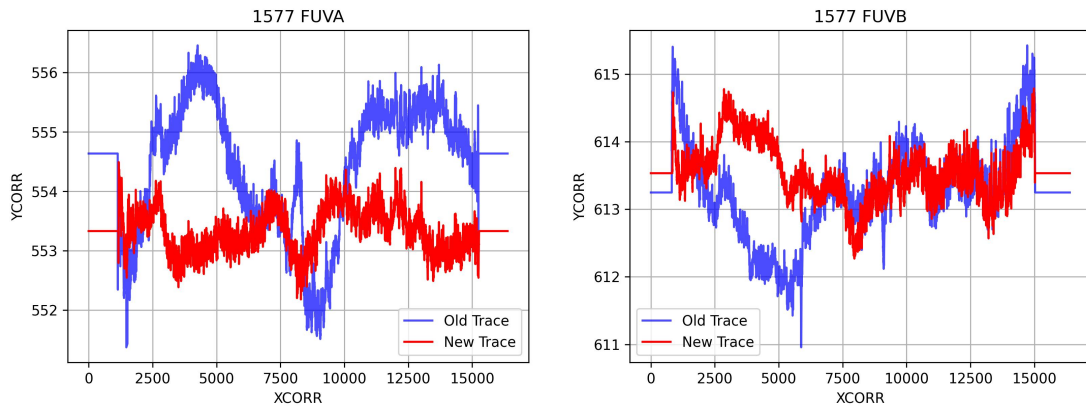


Figure 9. In each panel the two curves show flux-weighted centroids calculated for every XCORR column across the segment for observations made at LP6 with the G160M/1577 setting. Both curves were generated from analysis of the same observations, but the blue curve utilized data processed with the previous GEOFILE, while the red curve utilized data processed with the new dx and dy corrections. The left panel is for the FUVB segment using observations of the white dwarf WD 0308–565, while the right panel is for the FUVB segment using observations of the white dwarf GD 71.

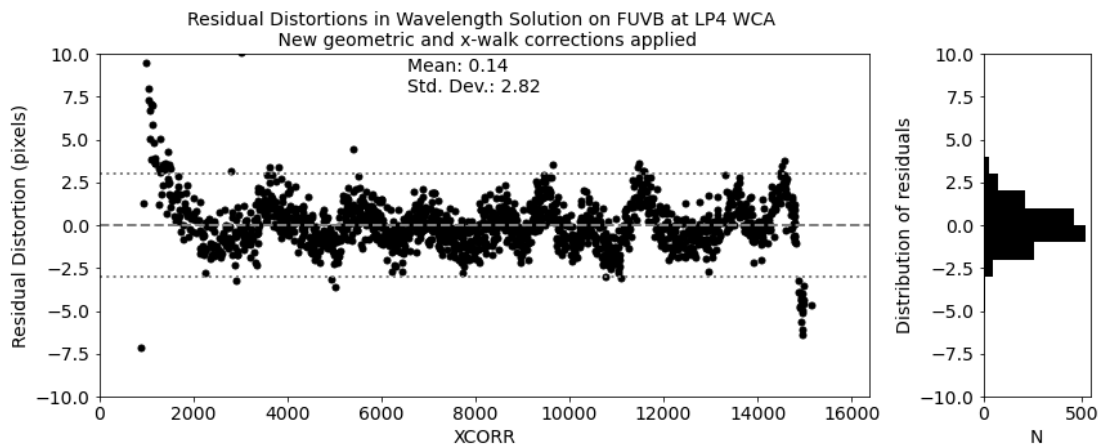


Figure 10. Residual shifts between measured and predicted locations for emission lines in spectra of the Pt-Ne hollow cathode lamp on the COS calibration platform, observed through the WCA. Both the new geometric distortion and X-walk corrections have been applied, and while the residuals are within the wavelength accuracy requirements, they clearly still show a pattern of coherent structures.

walk correction demonstrates that data products are significantly improved at all cross-dispersion locations on the detector where spectra are routinely observed.

Acknowledgements

The authors would like to acknowledge S. V. Penton, J. White, and D. Dashtamirova for their contributions to this effort while working at STScI.

Change History for COS ISR 2025-09

Version 1: 2 July 2025- Original Document

References

- Béland, S. & Penton, S. V. 2000 Bulletin of the American Astronomical Society, 33, 724, *In Preparation for the Cosmic Origins Spectrograph*
- Béland, S. & Penton, S. V. 2006, ADASS 351, 339, *Correcting for the Geometric Distortions on the COS FUV Detector*
- Béland, S., et al. 2003, TER COS-11-0044, *COS FUV Detector Geometric Distortion Maps*
- Béland, S., et al. 2007, COS-03-0090, *Generating the COS Reference Files*
- French, D., et al. 2025, COS ISR 2025-xx *Testing metrics* (In Preparation)
- Hasselquist, S., et al. 2024, COS ISR 2025-10, *Determining X-Walk Corrections for the COS FUV Detector*
- Hasselquist, S., et al. 2025, COS ISR 2025-11, *Determining Y-Walk Corrections for the COS FUV Detector*
- Indriolo, N., et al. 2025a, COS ISR 2025-07, *An Overview of Improvements to the COS FUV Geometric Distortion and Walk Corrections*
- Indriolo, N., et al. 2025b, COS ISR 2025-08, *Measurement and Implementation of a Delta-Geometric Correction for the COS FUV Detector*
- Osten, R., et al. 2013, COS ISR 2013-16, *Summary of Results from the First Move to a New COS FUV Lifetime Position*
- Sansonetti, J. E., Reader, J., Sansonetti, C. J., et al. 2003, *Atlas of the Spectrum of a Platinum/Neon Hollow-Cathode Lamp in the Region 1130-4330 Å* (version 1.2). [Online] Available: <http://physics.nist.gov/platinum> [2018, Jan. 23]. National Institute of Standards and Technology, Gaithersburg, MD.
- Soderblom, D., et al. 2022, *COS Data Handbook*, Version 5.1, (Baltimore: STScI).
- Vallerga, J. V. & McPhate, J. B. 2000, Proc. SPIE 4139, *Optimization of the readout electronics for microchannel plate delay line anodes*
- Vallerga, J. V., McPhate, J. B., Martin, A. P., et al. 2001, Proc. SPIE 4498, 141, *HST-COS far ultraviolet detector: final ground calibration*
- Wilkinson, E., Penton, S., Beland, S., et al. 2001, Proc. SPIE 4498, 267, *Algorithms for correcting geometric distortions in delay line anodes*
- Wilkinson, E., et al. 2008, COS-01-0008, *COS Prelaunch Calibration Data*

Wiza, J. L. 1979, Nuclear Instruments and Methods 162, 587, *Microchannel plate detectors*